Laboratory studies of thermally and/or salinity driven flows with partial mixing 1. Stommel transitions and multiple flow states

J. A. Whitehead,[1] M. L. E. Timmermans,[2] W. Gregory Lawson,[3] Sergey N. Bulgakov,[4] Alejandro Martinez Zatarain,[4] Jaime F. Almaguer Medina,[4] and John Salzig[1]

Received 2 April 2001; revised 30 August 2001; accepted 12 April 2002; published 18 February 2003.

[1] Laboratory studies with flows driven by both temperature and salinity differences illustrate the role of partial mixing in such flows. The results are compared to fundamental box model results. In the classic Stommel experiment, an experimental chamber is heated from below and exposed to a steady flux of salt water from above. The chamber is laterally connected to a reservoir of fresh isothermal water. This duplicates in part the well-known box models of deep ocean and estuarine circulation where both temperature and salinity determine the density in the chamber that drives a steady exchange flow between chamber and reservoir. Two locally stable modes of circulation are found within a well-known range of the temperature and salinity forcing: one mode is primarily temperature driven (the T-mode) and one mode is primarily salinity driven (the S-mode), with hysteresis and Stommel transitions between the two modes. New experiments with limited turbulent mixing and a narrow vertical slot in the sidewall between a laboratory test chamber and the reservoir produce a three-layer structure for the S-mode and a two-layer structure for the T-mode. Hysteresis and the Stommel transitions are considerably smaller than in the fully mixed box models. Results are consistent with the notion that the Arctic Ocean is presently in the layered S-mode. *INDEX TERMS:* 4203 Oceanography: General: Analytical modeling; 4263 Oceanography: General: Ocean prediction; 4568 Oceanography: Physical: Turbulence, diffusion, and mixing processes

Citation: Whitehead, J. A., M. L. E. Timmermans, W. G. Lawson, S. N. Bulgakov, A. M. Zatarain, J. F. A. Medina, and J. Salzig, Laboratory studies of thermally and/or salinity driven flows with partial mixing, 1, Stommel transitions and multiple flow states, *J. Geophys. Res.*, *108*(C2), 3036, doi:10.1029/2001JC000902, 2003.

1. Introduction

[2] The thermohaline circulation of the oceans is one of the classical subjects in Physical Oceanography. Observations indicate that the ocean salinity distribution may change significantly and alter global circulation over timescales from tens to thousands of years. *Broecker and Denton* [1989] showed evidence that glacial to interglacial transitions involve major alterations of the ocean's salinity distribution. Evidence cited includes the rapidity of glacial terminations, the hemisphere synchronicity and symmetry of mountain glaciation, and the large-scale variation of polar air temperature and dustiness. *Gordon* [1991] describes two stable modes of Southern Ocean water stratification. In one, referred to as the saline mode (S-mode), the sea ice cover and ocean stratification are maintained by salinity. In the other, referred to as the thermal mode (T-mode), the ice cover is absent and the mixed layer is great, from hundreds up to thousands of meters deep. *Weaver et al.* [1999] summarize the description of the thermohaline circulation in the Northern Pacific Ocean, which is more like the saline mode, and the North Atlantic Ocean, which is more like the thermal mode.

[3] This paper reports the results of a number of laboratory models of temperature–salinity driven flows. The models are designed to clarify the dynamics of water mass formation and thermohaline circulation in the world oceans and in buoyancy-driven estuaries. Even the simplest doubly driven problem has some complex behavior, as predicted in the seminal study by *Stommel* [1961]. He analyzed the exchange flow between two chambers of well-mixed water in a field of gravity, connected laterally by vertically aligned tubes. One of two distinct exchange states can exist when the chambers are exposed to both a heat and salinity flux. If the density difference between chambers arises predominantly from an increased temperature difference, the flow state is called a T-mode and if the density difference arises predominantly from an increased salinity difference, it is called an S-mode. Stommel showed that for certain forcing parameters either mode can exist and be locally stable. This

[1]Department of Physical Oceanography, Woods Hole Oceanographic Institution, Woods Hole, Massachusetts, USA.
[2]Institute of Theoretical Geophysics, DAMTP, University of Cambridge, Cambridge, UK.
[3]Massachusetts Institute of Technology, Cambridge, USA.
[4]Institute of Astronomy and Meteorology, University of Guadalajara, Guadalajara, Jalisco, Mexico.

Copyright 2003 by the American Geophysical Union.
0148-0227/03/2001JC000902$09.00

produces hysteresis, where the mode selected depends on the history of the experiment. In progressing from one mode to another, there is an abrupt change in flow direction and speed, a feature that is referred to as a "Stommel transition." These results have been verified by several numerical ocean models (summarized by *Marotzke* [1994], *Whitehead* [1995], *Hearn and Sidhu* [1999], and *Rahmstorf and Ganapolski* [1999]) and the Stommel transitions have been conjectured from indirect paleoclimate evidence. Physically, however, only a few measurements from laboratory experiments [*Whitehead*, 1996, 1998] support the existence of hysteresis and Stommel transitions. Both of these effects present difficulties for numerical modeling of the oceans and estuaries. For example, the modes may suddenly and catastrophically change from one to the other as external forcing parameters slowly change. As the parameters change back to their original values, the multiple equilibrium nature of the solutions means that the transition back to the original mode can happen at different parameters. In this case, the global thermohaline circulation depends upon history, and so too does the associated transport of heat from the equator to the pole and its consequent effect upon both regional and global climate. It is easy to visualize that, if a complicated ocean/atmosphere/climate model contains a number of regions where such hysteresis loops and their associated Stommel transitions arise as climate forcing changes, the forecasting problem could be complex indeed!

[4] The laboratory experiments discussed here do not have the numerous chambers and assorted atmospheric coupling processes found in numerical models, yet they do account for the added complexity of partial mixing. This is prompted by the fact that water mass thickness in the ocean is intimately connected to the rate of mixing, as recently illustrated by *Huang* [1999], and the measurement of mixing in the ocean continues to be a subject of active research [*Polzin et al.*, 1996, 1997]. Further motivation is that Stommel transitions and hysteresis have not yet been properly recognized in the ocean or in estuaries, so that direct observations of their physical effects, which have so many important implications for ocean climate, do not presently exist.

[5] This paper is outlined as follows. In section 2, studies of doubly driven flows with complete mixing are reviewed and some obvious qualitative effects caused by double diffusion in the channel connecting the laboratory chamber to the reservoir are described. In section 3, experiments and supporting theory for a system driven only by salinity flux and partial mixing are developed and analyzed. The effects of partial mixing are quantified and it is shown how partial mixing leads to one or two layers in the partially mixed chamber. In section 4, the laboratory experiments are designed such that the effects of both partial mixing and double driving are combined. Multiple equilibria and Stommel transitions are observed and described. The vertical salinity structure of the S-mode is markedly different to that of the T-mode. Furthermore, the range of hysteresis is considerably less than the box models. Results are summarized in the concluding section.

2. Doubly Driven Flow With Complete Mixing

[6] Consider first a laboratory chamber (Figure 1) in a field of gravity that is subjected to a flux of salt water

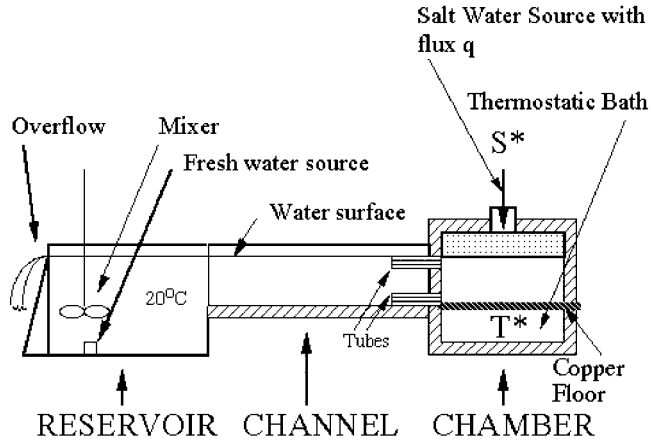

Figure 1. Sketch of the "inverse estuary" laboratory apparatus. Salt water of salinity S^* is pumped into the top of the chamber, which is heated from below at temperature T^*. Tubes at the top and bottom side of the chamber allow circulation into a channel. The other end of the channel is connected to a constant temperature freshwater reservoir on the left. The hatched region indicates thermal insulation.

pumped in from above while the chamber is heated from below through a thermally conducting bottom plate. The chamber is also connected laterally by two tubes in the sidewall to a narrow channel that leads to a reservoir filled with fresh isothermal water. The reservoir water is assumed to be renewed so that the temperature and salinity of the water remains constant in spite of an exchange flow between the reservoir and the chamber. This is called an "inverse estuary case," and the remainder of this section describes experiments with this configuration. The configuration differs from the "estuary case," to be considered in section 3, where the reservoir contains salt water representing the ocean, and freshwater is pumped into the chamber to represent river input. Note that, for a doubly driven estuarine case, the chamber may be additionally cooled from above to represent atmospheric cooling.

2.1. Theory

[7] Both the estuary case and its inverse obey similar dynamics, and transformation of dynamical equations between the two cases is straightforward. For sufficiently small volume flux of salt water into the chamber, the governing equations for deviations of salinity and temperature from a given reference state are [*Whitehead*, 1996]

$$\frac{dS}{dt} = \frac{1}{\tau_S}[S^* - S] - \frac{|Q|}{V}S, \tag{1}$$

$$\frac{dT}{dt} = \frac{1}{\tau_T}[T^{**} - T] - \frac{|Q|}{V}T \tag{2}$$

where Q is the volume flux of water from the reservoir to the chamber and V is the volume of the mixed water in the chamber. The time constants are given by $\tau_S = V/q$ and $\tau_T = [(k/\delta H\rho_0 C_p)) + q/V]^{-1}$, where salt water of salinity S^* (greater than the salinity of the reservoir for an inverse estuary, and less than the salinity of the reservoir for an

estuary) is pumped with volume flux rate q into the top of a chamber of depth H. The water has conductivity k, ρ_0 is the reference density of water taken to be the density of water in the reservoir, and C_p is specific heat. The boundary layer thickness δ is produced by cellular convection or mechanical mixing over the hot plate and is related to either Rayleigh number or Peclet number. The control parameter T^{**}, which will be varied in many of the experiments, is the temperature excess of the water in the copper chamber floor above the temperature of the reservoir water for the inverse estuary case. In the estuary case, which is not used in the present experiments, the control parameter T^{**} would be the temperature of the reservoir surface below reservoir temperature. The density of the mixed water in the chamber is taken to be a linear function of temperature and salinity. That is,

$$\rho = \rho_0[1 + \beta S - \alpha T], \tag{3}$$

[8] The doubly driven inverse estuary case will be the only case considered in the remainder of this section. Density deviates from the reference density due to the steady solutions to (1) and (2). For ocean problems, the usual approximation $1 < \beta S^*/\alpha T^{**} < \tau_S/\tau_T$ is valid. Consider for the moment that a small pump is used to drive the exchange flow between the small chamber and the reservoir and the above inequality is satisfied. The steady solutions relating flow, temperature and salinity given by

$$S = \frac{S^*}{1 + \frac{|Q|\tau_S}{V}} \tag{4}$$

$$T = \frac{T^{**}}{1 + \frac{|Q|\tau_T}{V}} \tag{5}$$

These are shown in Figure 2. For very small volume flux Q, the density deviation $(\rho - \rho_0)$ is positive and smoothly changes to a negative value as Q increases. For large values of Q, $(\rho - \rho_0) \rightarrow 0$. The sign of Q is irrelevant so that the same is true for negative Q. Upon removal of the pump, assume that the fluid in the chamber flows according to the relation

$$Q = C[\rho - \rho_0], \tag{6}$$

for a constant C. A line representing such a dynamical law governing flux through the channel is shown to intersect the density deviation curves in Figure 2. Three intersection points are shown, two stable fixed points (marked by circles) and one unstable one. The circles correspond to two stable "modes." The system could attain either one; hence, multiple equilibria are found. Note that this simple law, represented by a straight line, is only considered here for simplicity and other dynamical laws (see section 3) would be represented by curves. If such curves intersect the "sum" curve on Figure 2, they would also indicate more than one stable equilibria.

[9] A number of quantitative criteria have to be met in order to construct a laboratory experiment with such intersecting curves. Parameter values must lie in the range $1 < \beta S^*/\alpha T^{**} < \tau_S/\tau_T$ for the density deviation to change sign. In addition, the volume flux of water from the reservoir to the chamber must be sufficiently large compared to the volume of the mixed water in the chamber to produce a relation that intersects the curves at three points. If the flow through the channel is slow or the channel is very narrow, only the S-mode is possible, as shown by the steep straight line in Figure 2. This explains why marginal basins with narrow openings such as the Mediterranean Sea, the Black Sea, Chesapeake Bay and many estuaries have density fields dominated by salinity.

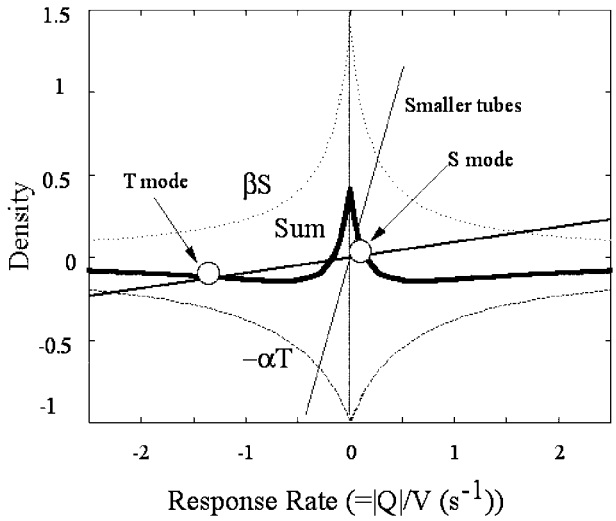

Figure 2. Curves expressing the behavior of Stommel's conceptual box model. The hyperbolae labeled βS and $-\alpha T$ are found ((4) and (5)) using a linear equation of state and parameters of the laboratory experiment. They indicate density deviations $(\rho - \rho_0)$ due to salinity and temperature, respectively. Their sum is shown by the dark curve. The dark straight line represents linear dynamics of flow. Intersection at the two circles gives two stable modes. The third intersection is unstable. For tubes with greater flow resistance (light straight line), only the S-mode is possible.

2.2. Experimental Results

[10] Experiments were conducted using two slightly different laboratory configurations. In one configuration, a well-mixed chamber was connected laterally to the reservoir by two tubes, one upper and one lower. This is identical to the configuration used by *Whitehead* [1996, 1998]. In the second configuration, shown in Figure 1, the two side tubes were connected to a long channel to join the chamber to the reservoir. The purpose of the channel modification was to conduct additional experiments to assess the role of molecular diffusion in the connecting channel [W. G. Lawson, Summer student report, Woods Hole Oceanographic Institution, Woods Hole, MA, unpublished, 1997]. The results of the experiments with the channel will be described in the latter half of this section. In both configurations, the experimental parameters are identical to those used in previous experimental studies [*Whitehead*, 1996, 1998]. The thermal constant of this chamber is about $\tau_T \approx 500$ s and the salinity time constant is about $\tau_S \approx 1500$ s.

[11] Figure 3 presents the results for both configurations (with and without the channel) in a form familiar to physical oceanographers. Results from both configurations agree with

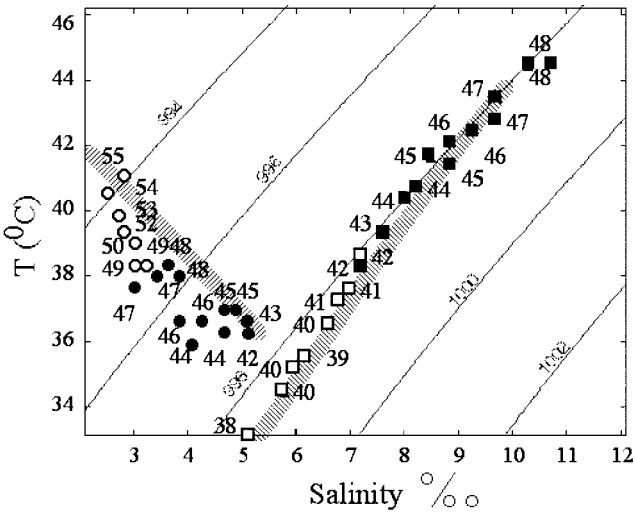

Figure 3. A *T*/*S* diagram showing experimental values of the salinity and temperature of water in the chamber in a range of multiple equilibria laboratory experiments where the external volume flux *q* and salinity *S** are held constant while *T** is varied. Contours indicate density (in MKS). The squares indicate mixed-water properties when the system is in the S-mode, and the circles when it is in the T-mode. The solid symbols denote the points with two stable modes. The value of *T** is shown next to each symbol, located to the right for experiments with a channel and to the left without the channel. The hatched broad lines are theoretical predictions using (3)–(6).

the simple box model theory and show multiple equilibria. The symbols show that for *T** below about *T** = 48°C, flow entered the chamber through the top tube and exited through the bottom tube (i.e., the flow was in the S-mode). For values of *T** above about *T** = 42°C there were other runs where flow entered the bottom tube and exited the top tube (i.e., it was in the T-mode). These results show that Stommel transitions are found near *T** = 42°C and *T** = 48°C with hysteresis in between these values. Theoretical predictions using (1)–(3) with values for the experiments are shown as the two hatched lines in Figure 3. The experiments reproduce a number of features predicted by the simple theory. The trajectory of points in *T*–*S* space tracks the isopycnal of freshwater at room temperature as *T** approaches the upper transition value $T^* \rightarrow 48°C$ when the system is in the S-mode. The theoretical predictions (Figure 2) indicate that, as this limit is approached, the volume flux between the reservoirs goes to zero as observed in the experiments. Unlike the theory, the full equation of state for salt water [*Fofonoff and Millard*, 1983] was used for the contours in Figure 3. Comparison with sodium chloride tables revealed that the difference in chemical composition between the international standard seawater and pure sodium chloride does not effect density to the level considered in this study. The critical values of temperature and salinity inside the chamber are predicted from the equations to be *T* = 44°C and S = 10.3‰. These values are close to those found experimentally as shown in Figure 3. However, the experimental value of the control parameter is *T** = 48°C, a fact not in accord with the theory and possibly due to heat loss in the apparatus. Finally the values of the properties for the case $\beta S^* = \alpha T^{**}$ can be readily calculated from theory. In this case, the value of density difference from the reservoir water is obtained by setting the derivatives of density with respect to volume flux for salinity and temperature equal to each other. This yields the minimum possible density difference between chamber and reservoir as $\rho_0 \beta S^* \left[\left(1 - \sqrt{\tau_S/\tau_T}\right)/\left(1 + \sqrt{\tau_S/\tau_T}\right)\right]$ which for the experimental parameters is 2.0 kg m^{-3} giving a possible value of density of 996 kg m^{-3}. The value of density in Figure 2 lies slightly below this value for *T** = 49°C. The corresponding value of transition salinity is $S = S^*/\left(1 + \sqrt{\tau_S/\tau_T}\right)$ = 3.8‰ which is about 25% above the value 3.0 for *T** = 49°C. In addition, it can be shown that for the T-mode just above transition for the parameters of this experiment the relation $\alpha \partial T/\beta \partial S = -1$ holds. This slope is approximated reasonably well by the data. Finally, the solid curves show the trajectory of the theoretical solution using the parameters of this experiment. In summary, the data and the curves show good, but not precise agreement both with and without the channel.

[12] Experiments conducted with the apparatus of Figure 1, in which a channel connects the chamber to the reservoir, revealed a three-layer flow in the channel, irrespective of whether the chamber was in the T-mode or the S-mode [Lawson, unpublished, 1997]. At the reservoir end of the channel, there was flow from the reservoir into the channel at middepth and flow from the channel to the reservoir at both the top and the bottom of the channel. Double-diffusive effects [*Schmitt*, 1994] were most likely responsible for generating this three-layer flow. When the chamber was in the T-mode, the outflow from the chamber through the top layer was warmer than the reservoir water. This outflow released heat to the ambient water in the channel and the cooled salty water was observed to sink to the floor of the channel in salt finger cells. The heated fresh (ambient) water exited the channel along the top and the cooled salty water exited along the bottom. There was an inflow at middepth. This inflow supplied water to be heated by the fingers, and also to be entrained into the fingers from the change in salinity due to the diffusion of salt. Conversely, if the chamber was in the S-mode, the hot, dense, salty water entered the bottom of the channel from the bottom tube of the chamber. The layer of dense water released heat to overlying ambient water that rose in thermal convection cells and gathered at the top of the channel. As in the T-mode, both the top and the bottom layers flowed out of the channel with inflow in the middle. Again, the inflow was assumed to resupply the heated water. In spite of these complex flows in the channel, the measured results (shown in Figure 3) were similar to the earlier experiments without the channel. These results suggested that experiments in which a continuous slot opening replaced the two overlying tubes would be of interest.

3. Quantifying Mixing Rate

[13] Exploratory experiments were conducted with a similar apparatus to that in Figure 1, with a vertical slot opening in place of the two tubes. Visual observations revealed that the interior of the chamber assumed layers at times, while at other times layers were not observed. The layers in these exploratory runs may or may not be similar

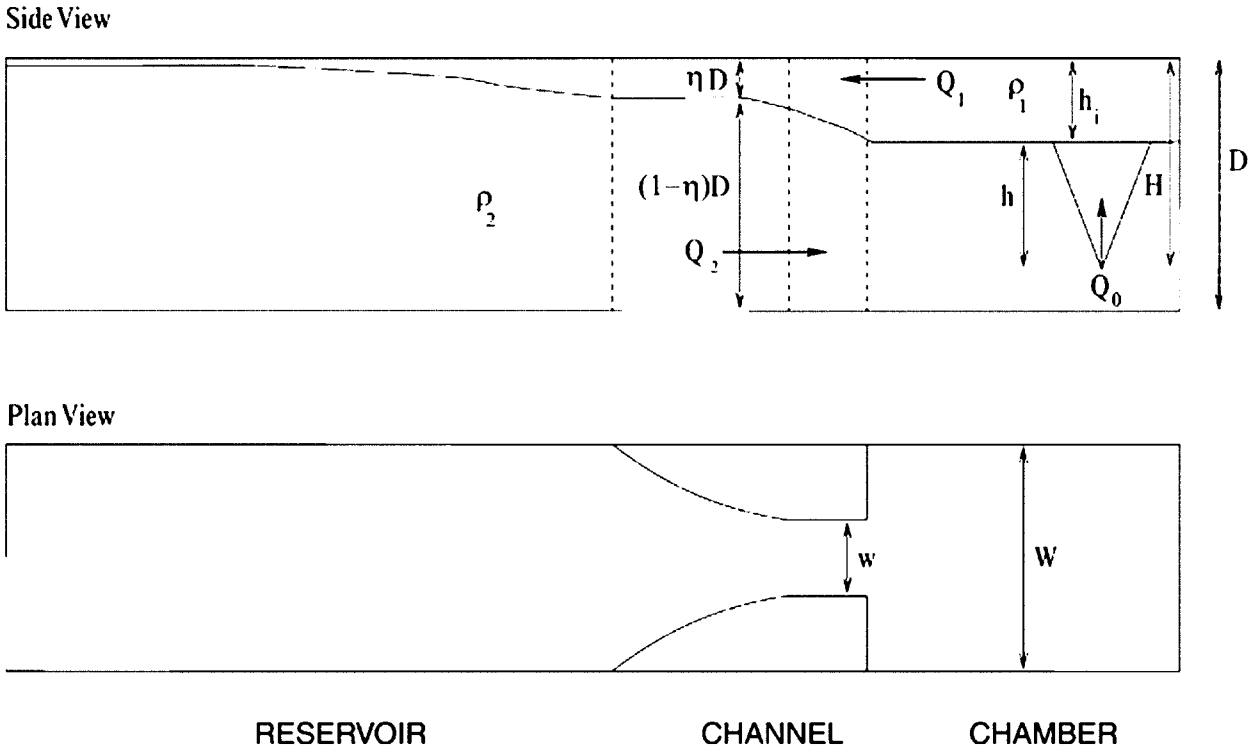

Figure 4. The apparatus used to study the estuary case of exchange flow with partial mixing. Freshwater influx into the salt water surroundings and mixing in the smaller chamber results in a flow of lighter mixed water, of density ρ_l, out of this reservoir in an upper layer, of thickness ηD, in the channel. A relatively dense (density ρ_2) inflow in a lower layer of thickness $(1 - \eta)D$ is exchanged. This inflow comes from the larger reservoir to the left.

to the double-diffusive layers in the channel described above. Hence, a method was devised to provide some quantified mixing inside the chamber to determine the origins of the observed layers. In this section, experiments with only salinity forcing are described and an associated theory is developed to quantify the effects of mixing. The results presented here follow from initial studies of partially mixed, hydraulically controlled exchange flows [*Timmermans*, 1998]. The work extends a study of "overmixed" estuaries [*Stommel and Farmer*, 1952, 1953], where the density difference between two layers in an ocean–estuary exchange is a minimum. Other related experiments have, for example, the sources distributed along the top surface in conjunction with exchange flow [*Brocard and Harleman*, 1980, also *Grimm and Maxworthy*, 1999]. This study varies from previous experiments mainly in that a point source of buoyancy (a plume) is used, rather than a distributed source, to simulate mixing. Hence, well-established plume theory can be used to explicitly quantify mixing.

3.1. Partially Mixed Exchange Flows

[14] In this section, experiments and theory using an estuary configuration are discussed. A steady, frictionless two-layer flow in a channel between a small chamber and a larger reservoir is considered. The apparatus and variables are shown in Figure 4.

[15] The large reservoir contains well-mixed salt water and represents the deep ocean. A steady flux of freshwater, representing the influx of river water, is pumped in through a small source at fixed depth in the chamber. A river introduces freshwater at the surface but it is also subjected to wind and tidal mixing. The laboratory source is placed at some depth to model such mixing. This freshwater rises from the source as a buoyant plume, entraining the ambient salt water in the chamber, so that the depth of the source determines the mixing between the fresh and salt water. The mixing drives a two-layer exchange flow through the channel. The conservation of volume flux is given by $Q_1 - Q_2 = Q_0$ where the subscript 0 refers to the water introduced from the exterior into the chamber, and subscripts 1 and 2 refer to the upper and lower layers in the channel respectively. All values are positive so that the upper-layer flow is out of the chamber and the lower-layer flow and freshwater flux are into the chamber. Conservation of salinity s is given by $Q_1 s_1 - Q_2 s_2 = 0$. A lower case s is taken to refer to salinity in these estuary studies, while an upper case S refers to salinity in the doubly driven experiments.

[16] We assume that the flow is critically controlled at the narrowest point in the channel so that the composite Froude number is unity [*Stommel and Farmer*, 1952; *Armi and Farmer*, 1986]. That is, in the Boussinesq approximation $F_1^2 + F_2^2 = 1$, where $F_n^2 = \frac{u_n^2}{g' d_n}$ is the square of the internal Froude number of layer n, which has thickness d_n, speed u_n and volume flux $Q_n = u_n d_n w$ through the channel of width w. The reduced gravity between the two flowing layers is given

by $g' = g\beta(s_2 - s_1)$. The quantities are nondimensionalized as follows: widths by w, vertical distances by the total depth D of the connecting channel and volume fluxes by $g_0'^{1/2}D^{3/2}w$, where $g_0' = g\beta s_2$ is the reduced gravity of the unmixed salt water. A fraction η is introduced such that the layer thicknesses are given by $d_1 = \eta D$, $d_2 = (1 - \eta)D$ (the deflection of the free surface is negligible compared to the total fluid depth). The critical condition may now be expressed in terms of dimensionless variables as,

$$\frac{1}{\eta^3} + \frac{(\tilde{g}' - 1)^2}{(1-\eta)^3} - \frac{\tilde{g}'^3}{\tilde{Q}_0^2} = 0, \tag{7}$$

where the tilde over a quantity signifies that it is nondimensional, and $0 < \tilde{g}' = \frac{g\beta(s_2 - s_1)}{g\beta s_2} < 1$. This is the range between completely mixed and not mixed at all.

[17] Turbulent buoyant convection from a point source of freshwater is used to generate vertical mixing in the chamber. Hence, the amount of mixing may be progressively increased by extending the distance over which the buoyant plume moves vertically, thereby increasing the amount of entrainment of salt fluid into the fresh plume. An axisymmetric plume is generated by an idealized point source of buoyancy in stationary fluid far from the channel, for which buoyancy flux $B_0 = Q_0 g_0'$ remains constant. Soon after the freshwater flux into the small chamber is initiated, a steady state is achieved in which a mixed layer of uniform thickness $\tilde{h}_i$ accumulates at a distance $\tilde{h}$ above the source. Let $\tilde{H}$ be the nondimensional depth of the source below the water surface so that $\tilde{h} = \tilde{H} - \tilde{h}_i$. Basic plume theory yields the reduced gravity between the upper mixed layer in the chamber and the underlying salt water. That is [*Morton et al.*, 1956],

$$\tilde{g}' = \left(\tilde{Q}_0 w/D\right)^{2/3} / c\left(\tilde{H} - \tilde{h}_i\right)^{5/3}, \tag{8}$$

where c is an empirical constant, found to be approximately 0.12 in experiments. The density of the mixed layer is equal to the density of the plume fluid at the interface between the two layers. Furthermore, the vertical volume flux in the plume at the mixed-layer depth is equal to the volume flux in the top layer through the channel plus the volume flux of the source.

[18] Equation (8) introduces a new variable $\tilde{h}_i$ so that an additional relationship between $\tilde{h}_i$, η, and $\tilde{g}'$ is required. This equation is obtained by applying Bernoulli's principle along two streamlines just above and below the interface between the two layers. That is,

$$P_i + \rho_1 g(D - h_i) = 1/2\rho_1 u_1^2 + P_c + \rho_1 g(1-\eta)D,$$
$$P_i + \rho_2 g(D - h_i) = 1/2\rho_2 u_2^2 + P_c + \rho_2 g(1-\eta)D,$$

where P_i is the pressure on the interface at the level $\tilde{h}_i$ and P_c is the pressure in the narrowest part of the channel on the interface at the level ηD. The left sides of these expressions apply in the chamber far from the plume where the flow is negligible and the right sides apply at the narrowest section in the channel. Further, it is assumed that the chamber is much wider than the channel, and there is no change in energy before and after the transition in width. Taking the difference of these two equations and scaling as before yields

$$\frac{1}{\eta^2} - \frac{(\tilde{g}' - 1)^2}{(1-\eta)^2} + \frac{2\tilde{g}'^3}{\tilde{Q}_0^2}\left(\eta - \tilde{h}_i\right) = 0 \tag{9}$$

The derivative of this with respect to η is the control equation (7). Equations (7)–(9) must be solved numerically for η, $\tilde{g}'$, and $\tilde{h}_i$. Analytical solutions can be found in the limits of large and small mixing . The overmixed solution of minimum g' is given by $\tilde{g}' = (\tilde{Q}_0^2/\eta^4)^{1/3}$ and, in this limit, for small $\tilde{Q}_0$,η = 1/2 [*Stommel and Farmer*, 1953]. For small mixing, in the limit of $\tilde{g}' \to 1$, $\tilde{h}_i = 3\eta/2$.

[19] A test of the theory was carried out in a laboratory flume 4.6 m in length, 0.6 m high, and 0.4 m wide, filled with ocean salt water. The channel was a Perspex contraction in the flume so that the length of the small chamber was 0.4 m long and the reservoir was 4.2 m long. The contraction was abrupt on the side joining the chamber, where it had a width of 0.05 m. The clear flexible plastic channel walls widened over a length of 0.4 m onto the side of the larger reservoir. The initial reduced gravity g_0' between the freshwater and the salt water was 0.23 m s^{-2}.

[20] Experiments were initiated by releasing freshwater from an upward pointing tube in the chamber placed at some depth H under the saltwater surface. In order to increase the volume flux through the contraction for the same buoyancy flux, experiments were also performed with a varying number of sources placed at the same vertical level. The total buoyancy flux from the source or sources was $B_0 = 1.6 \times 10^{-6}$ m^4 s^{-3} for all runs, for purely buoyancy-driven plumes. The fresh fluid ascended within a turbulent entraining plume and accumulated in a layer of mixed water at the top, driving an exchange flow through the contraction. Approximately 1–2 min after the freshwater flux was initiated, a steady state two-layer system was observed. The two layers were visualized by adding dye to the freshwater supplied at the source. Water samples, taken to measure the density of the surface mixed layer, indicated that it was well mixed. Once this steady state was reached, the exchange flow was observed for various values of H; a total of 20 runs were conducted with varying values of H. The same plume source, of diameter 0.01 m, was used each time.

[21] Experimental measurements of the three unknowns are shown (Figure 5) as a function of the amount of mixing (i.e., $\tilde{H}$), for which it was necessary to determine the position of the virtual point source below the nozzle opening. Numerical solutions to (7)–(9) are shown by the curves. The experimental results show how very small mixing $\tilde{g}' \to 1$ was difficult to achieve in the laboratory, although η and $\tilde{h}_i$ show agreement with the one-layer relationship ($\tilde{h}_i = 3/2\eta$). As the overmixed limit is approached ($\eta \to 1/2$), the mixed-layer thickness $\tilde{h}_i$ in the chamber does not lie on the numerical curve. This disagreement is a result of the incorrect assumption that the exchange flow is nondissipative in a well-mixed chamber, a point that is well known [*Stommel and Farmer*, 1953]. In addition, the overmixed limit is a special case that is separated from supercritical flows by a discrete jump in properties [*Armi and Farmer*, 1986]. In any event, beyond the overmixed state, the present theory can no longer predict the height of the

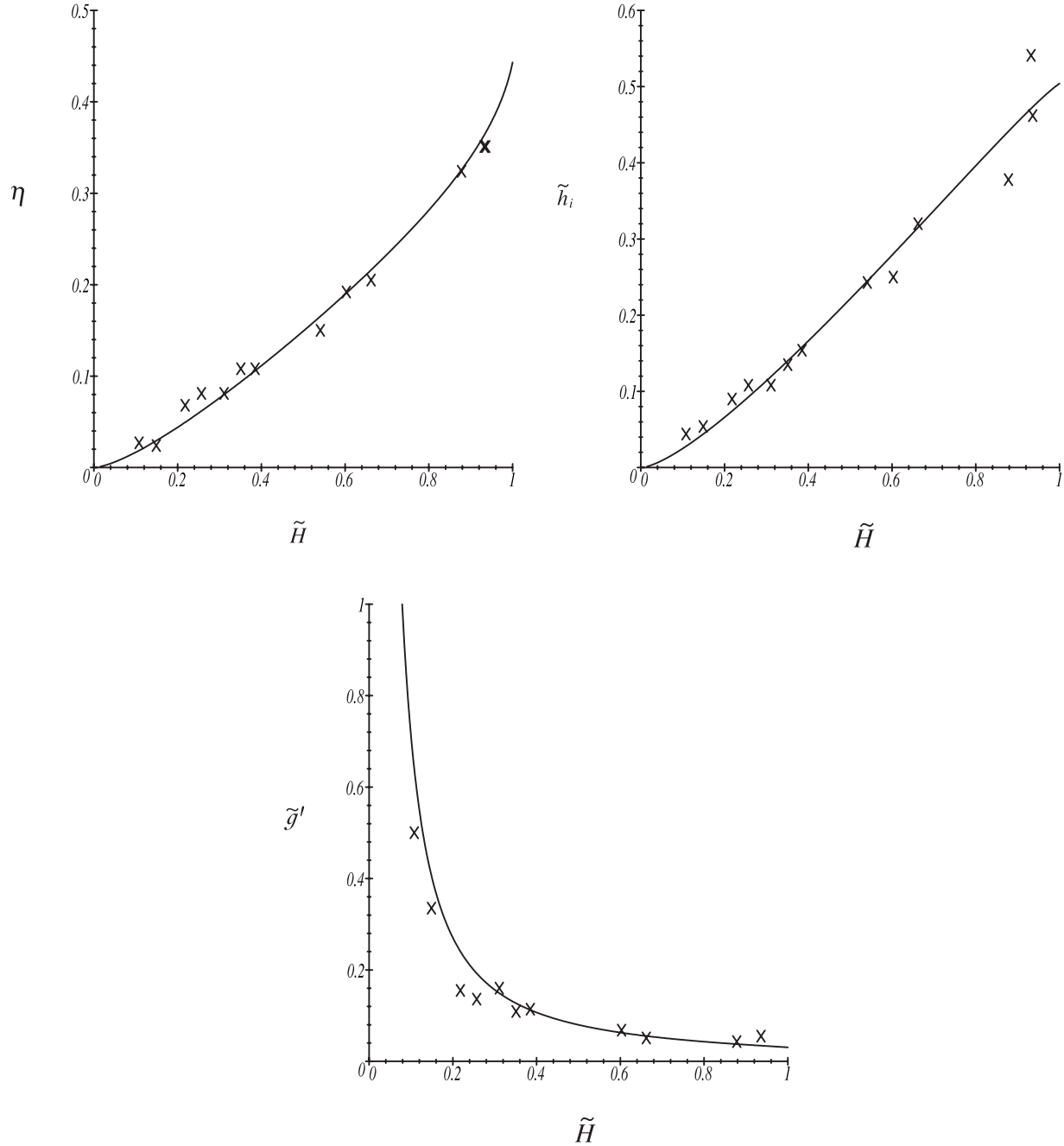

Figure 5. The relationship between the dimensionless depth $\tilde{H}$ of a single freshwater source and (a) the mixed-layer thickness η in the contraction, (b) the mixed-layer thickness $\tilde{h}_i$ in the chamber, and (c) the reduced gravity $\tilde{g}'$. The curves are the numerical solutions (c = 0.22) and the crosses are experimental results.

interface in the chamber. Experiments with multiple plumes also exhibited wide scatter near the overmixed limit.

3.2. The Overmixed Limit

[22] The proceeding apparatus was limited to the values $\tilde{H} < 1$. An experimental configuration used to obtain larger $\tilde{H}$ is sketched in Figure 6. The channel was smaller in vertical extent with a square (0.1 × 0.1 m) cross section and it was fixed near the bottom of a vertical wall separating a small chamber (1 m long) from a large reservoir (4 m long). The level floor of the channel was 0.05 m above the chamber and reservoir bottoms. To avoid some flow separation that was observed in preliminary experiments, both ends of the channel were flared to a final width of 0.2 m wide and 0.2 m high. The lateral length of each flare was 0.2 m span. The plume source was a metal tube (0.0073 m inner diameter) pointed downward with $\tilde{g}_0' = 0.22$ m s^{-2} and $Q_0 = 7.33 \times 10^{-6}$ m^3 s^{-1} (giving $B_0 = 1.64 \times 10^{-6}$ m^4 s^{-3} and $\tilde{Q}_0 = 4.9 \times 10^{-3}$). The range investigated was $0 < \tilde{H} < 5.0$. The pumping rate, the density difference between the input and chamber fluids, and the input tube diameter were equal to the parameters in section 3.1 so that the plume had the same

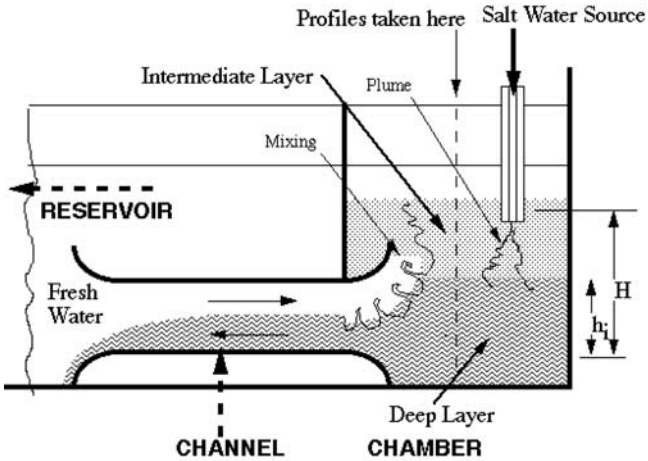

Figure 6. Sketch of the apparatus to investigate very large mixing.

Reynolds number. However, since the channel depth D is less than before, the scaled influx $\tilde{Q}_0 = 4.9 \times 10^{-3}$ is different although it is still sufficiently small that the small flux approximation of section 3.1 is still valid. That is, the barotropic flux out of the small chamber is small compared to the baroclinic flow for all parameters. Using (8) and the overmixed limit with $w = D = 0.1$ m, the plume level for overmixing is predicted to be $\tilde{H}_{ov} = 2.5$.

[23] As in the previous experiments, a run commenced with the initiation of the pump that supplied the salt water. Measurements of the density distribution in the small chamber were made using a salinity microprobe that was lowered vertically with a stepper motor. Including exploratory runs, a total of 59 density profiles were taken to determine response times of density and flows in the small chamber. The output was calibrated using water samples taken at selected locations. Density of these samples was determined to five decimal places using a precise densiometer. The salt water pumped in contained dye so that the water and any mixture could be seen by eye. Vertical columns in the channel were observed by dropping potassium permanganate crystals through holes at three locations in the channel. The velocity from the column deformation had a well-developed profile. This indicated that the flow possessed developing boundary layers at the walls. In addition, waves were seen on the interface between the two layers in the channel. Both indicate that inviscid dynamics, expressed by (9), are violated by the channel flow.

[24] Figure 7 shows the 14 final steady state profiles for experiments with 6 different values of $\tilde{H}$. Since the small chamber's floor is slightly deeper than the floor of the channel, profiles were extended below the channel floor depth. Depth $\tilde{z}$ is scaled by channel depth D. To verify the steady nature of the final fields, a series of earlier density profiles (not shown) were measured at time intervals longer than 15 min. For the cases of very large mixing, the density field took up to 2 hours to achieve steady state. This time is very much longer than the experiments in section 3.1.

[25] The characteristic two-layer profile of the undermixed state was observed for runs with $\tilde{H}$ = 1.5, 2.0, and 2.5. That is, the interface elevation lay roughly at or below the middepth of the channel $\tilde{z} = 0.5$ The overlying layer had a density that was close to that of the water in the large reservoir. The density difference between the two layers was greater than the overmixed value, as discussed in section 3.1. For $\tilde{H}$ = 3.0, 4.0, and 5.0, the interface lies at about $\tilde{z}$ = 1.0, 1.5, and 2.0 respectively. Above this, there is a transition region ($\Delta\tilde{z} \sim 0.2$) to a second layer of constant intermediate density that extends up to about $\tilde{z}$ = 3.0, 3.5, and 5.5, respectively. This second layer was overlain with freshwater. The elevation of the top of the second layer was close to the elevation of the source.

[26] The observed layer of intermediate water between $2.0 < \tilde{z} < 5.5$ was not anticipated. It can be seen in a photo of the experiment (Figure 8) as a thick layer of intermediate gray above the black bottom layer. It contains a mixture of freshwater that entered the small chamber along the top half of the channel and salty water from the well-mixed lower layer. The mixing source was twofold. First, very obvious roll waves were located along the interface of the freshwater flowing into the small chamber in the flared region. These are shown in the close-up photograph of the channel entrance in Figure 9, and they are very visible in videos of the experiment. Second, the rapidly rising freshwater mixed energetically with the lower water by entraining lower-layer fluid while rising through it toward the top of the small chamber.

3.3. Theory and Quantitative Results

[27] For large $\tilde{H}$, the mixed layer in the small chamber is deeper than the overmixed layer depth, so that $\tilde{h}_i > 1/2$. The experiment showed shear instability present at the inflow to the small chamber. The incoming fluid thereby mixes and acquires a salinity change. This mixing may be a sensitive

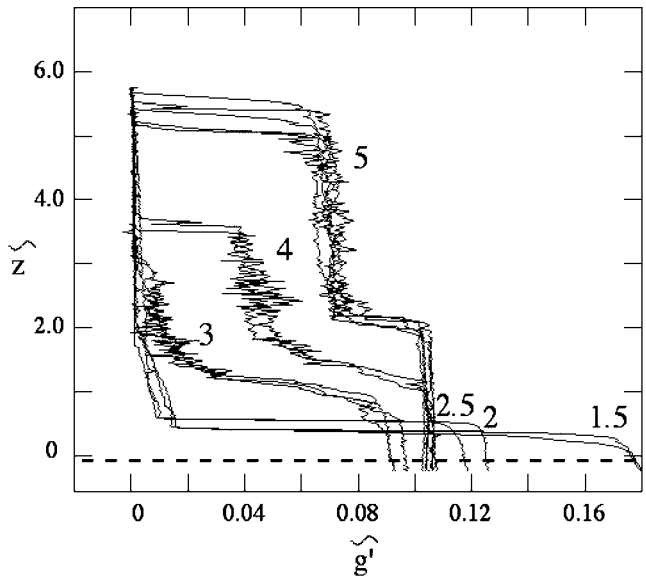

Figure 7. Density profiles after the experiment sketched in Figure 6 has achieved a steady state. The numbers near the curves denote values of $\tilde{H}$. The vertical scale $\tilde{z}$ has been nondimensionalized by the channel height D = 0.1 m. The dashed line and the vertical origin give the level of the floor of the channel. Assorted profiles for the same values of $\tilde{H}$ were taken more than 5 min apart.

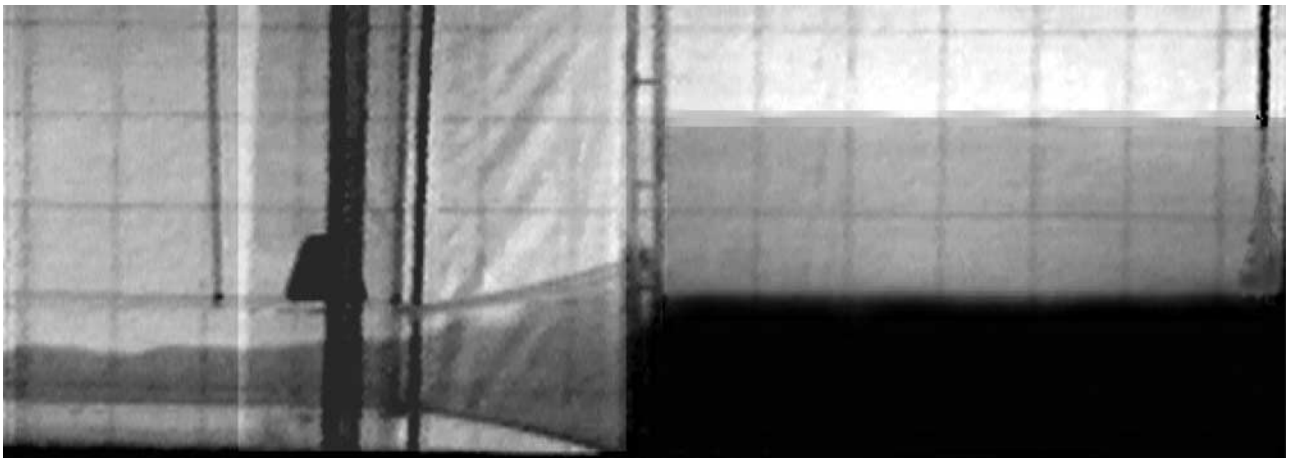

Figure 8. Side view of the experimental chamber (sketched in Figure 6) with $\tilde{H} = 3$. The small chamber occupies the right side of the image. The source can be seen at the far right as a vertical black tube, below which the plume is visible. Two layers occupy the chamber. The deepest is black and contains the salty water exiting the chamber. The middle layer is light gray and extends up to the level of the tube outlet. The channel is in the lower left of the photograph. Dyed salty water is flowing out toward the left and clear water is flowing into the small chamber above it.

function of geometric factors in the flared channel region. Nevertheless, the plume equation (8) can be modified to incorporate an ambient salinity by simply imposing a background salinity of unknown magnitude in the small chamber. The equivalent equation is

$$\tilde{g}' - \hat{g}' = c^{-1}\left(\tilde{Q}_0^2\left(\frac{w}{D}\right)^2\left(\tilde{H} - \tilde{h}_i\right)^{-5}\right)^{1/3}. \qquad (10)$$

[28] This equation has two additional unknowns, scaled ambient density of the intermediate layer $\hat{g}'$, and distance from the source to the interface between the bottom and intermediate layers $\tilde{H} - \tilde{h}_i$. Here it is assumed that $\hat{g}' \ll 1$, so that the buoyancy flux of the source is not modified by the background salinity. The mixing in the shear instability/hydraulic jump region, shown in Figure 9 must relate $\hat{g}'$ and $\tilde{h}_i$, but that relation is likely to be dependent on the detailed geometry of the region. Equation (10) can be tested using measured values of the density of the intermediate layers and values of $\tilde{h}_i$ directly from Figure 7. Figure 10 shows the results for the three highly overmixed experiments. The average of the numerous profiles shown in Figure 7 is incorporated in this figure. The trend follows a reasonably

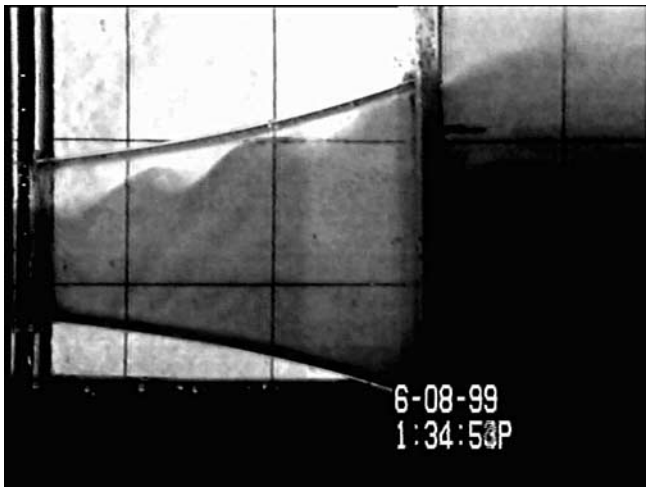

Figure 9. Side view of the flared entrance region of the small chamber, which lies to the right. Roll waves and overturning eddies mix dyed salty water into the clear freshwater as it enters the small chamber. This mixing produces the intermediate layer visible in the upper right corner.

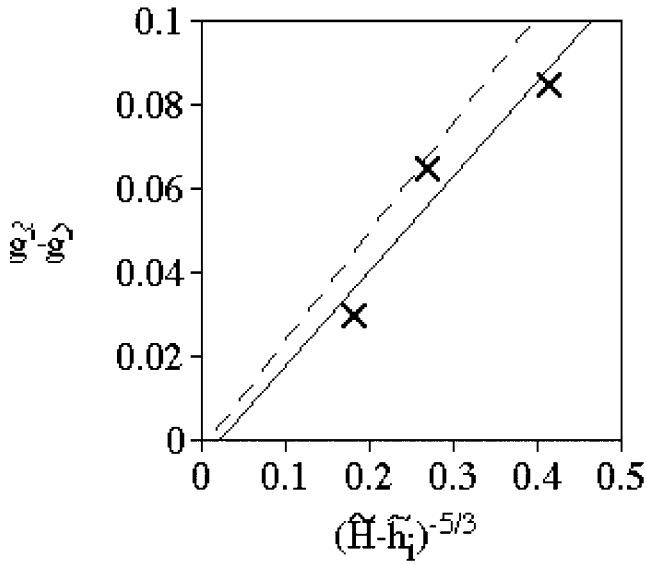

Figure 10. Density difference for runs with $\tilde{H} = 3$, 4, and 5. The dashed curve is the theoretical curve (10) using the parameters of the experimental system. The best-fit straight line is given by $\tilde{g}' - \hat{g}' = 0.23(\tilde{H} - \tilde{h}_i)^{-5/3} - 0.005$.

straight line, with a constant for the best fit of 0.23 ± 0.05. The slope from (10) is 0.25 using the experimental values of $\tilde{Q}_0$, w, D, and c which is close to the theoretical curve. Thus, the intermediate layer provides the necessary salt flux into the plume to bring the lower-layer salinity to the required value for the salt to be removed by flow at the overmixed rate.

[29] There is evidence that frictional drag is significant along the 1.0 m long channel. First, images reveal a systematic tilt of the interface in the channel of more than 1 part in 10 (partially visible in Figure 8). Since the channel is carefully leveled and exactly the same height over its length, this tilt must be due to a change in pressure along the channel. This pressure gradient evidently arises from developing viscous boundary layers on the four sides of the channel. Second, the value of $\tilde{g}'$ is predicted to be 0.073 in the overmixed limit using (10), but the experimental value for the minimum density difference is closer to 0.086.

3.4. Interpretation of the Results

[30] In order to quantify the role of mixing in these experiments, the hydraulics of undermixed inertially controlled flows was combined with plume theory to investigate the effects of mixing rate upon the strength of circulation. The purpose of using plumes in this model is primarily to have a well-known mechanism in the dynamics of mixing, and the results do not depend in detail upon the nature of plume theory. Any number of other mechanisms for mixing the layer of water in the small chamber would also work. For example if a jet of water of differing salinity were to be placed in the small chamber to produce mixing, the kinetic energy flux of the jet would supply the power of mixing. Alternately, if the mixing were provided by a moving grid [*Turner*, 1973], the power required to move the grid would be comparable to the plume power.

[31] Overmixing occurs for $\tilde{h}_i > 0.5$, while experiments in this section show that the freshwater flowing into the small chamber mixes with the deep layer to form another layer. The situation is in fact observed in the Black Sea, a very large estuary case, where rivers supply freshwater and there is an exchange flow with the salty Mediterranean Sea through the Bosporus. The halocline (thus, pycnocline) depth of the Black Sea is about 100 m. This is much greater than the channel depth of about 40 m. The high salinity water from the Mediterranean flows into the Black Sea along the bottom of the Bosporus and descends as a small turbulent current [*Ozsoy et al.*, 1993] that mixes with the freshwater above the halocline. Thus the salinity of the deep Black Sea is only about 22 parts per thousand compared to about 38 parts per thousand for the Mediterranean [*Sverdrup et al.*, 1942, Tables 79 and 80].

[32] Experiments with grid mixing in assorted different locations would likely show that the location of mixing is also important. Oceanographers are currently discovering this fact in the Atlantic [*Polzin et al.*, 1996, 1997]. For example, in the estuary case, if a grid mixer were placed deep in the salt water of the small chamber with freshwater pumped in at the top, the entrainment velocity of the interface would be directed upward, since entrainment velocity is always directed away from the water with most energetic turbulence [*Turner*, 1973]. However, since the thin layer of freshwater is located along the top surface, the interface would be forced to remain there. Some freshwater would be entrained into the deep salt water and it is likely that an overmixed exchange flow would result through the channel for all mixing rates.

[33] The salt water experiences a change in potential energy as it descends from the source. The rate of change of potential energy, or power released is

$$P_s = \rho_0 Q_0 \left[g_0' H - g' h_i \right]. \tag{11}$$

The power required to elevate the salt water from the bottom of the tank to the midpoint of the mixed layer is

$$P_l = \rho_0 Q_0 \left(g_0' - g' \right) [h_i/2]. \tag{12}$$

Hence, the net power that is released by the plume of descending salt water from the source to the mixed layer is $P_s - P_l$. In section 3.1 (the estuary problem), the balances are the same. In that case, the power P_l is dissipated in moving the freshwater up to the top mixed layer out of the small chamber. A mechanical mixer would have to be driven by more than this power to produce the same amount of mixing.

[34] In the ocean, there are many sources of mixing including tides, currents from wind driving, and breaking internal waves. The minimum power required (without frictional losses) for vertical mixing in the global ocean could be estimated from (11). Using a 10° temperature difference $g_0' - g' = g\alpha\Delta T = 2 \times 10^{-2}$ ms $\rho_0 = 1000$ kg m^{-3}, a volume flux consistent with deep water production of about $Q_0 = 10^7$ m^3 s^{-1}, and a deep thermocline value $h_i = 1000$ m, it can be deduced that $P_l = 10^{11}$ W. Since h_i is 20% of the depth of the ocean, the oceans are undermixed. The results in Figure 5b indicate that, over a wide range of values, $\tilde{h}_i/\tilde{H} \sim 0.5$ which, with (11) and (12), implies that $P_l/P_s \approx 0.25$ and thus $P_s = 4 \times 10^{11}$ W. *Huang* [1999] indicates that the rate of tidal dissipation in the deep ocean is about 2 or 3 times greater than this value. Thus, the rough estimates here lie within factors of 2 or 3 of values based on direct ocean observation.

[35] These results are consistent with *Huang*'s [1999] assertion that the mixing source is actually the source of energy that drives the exchange flow. This point is clear from the simple plume model, while for general sources of turbulence in the ocean, it is not as obvious that the turbulence produces the potential energy for the flow. The production of potential energy by oceanic turbulence and its role in general ocean circulation was pointed out by *Faller* [1966] and developed further by *Huang* [1999]. Huang describes how the concept has been discussed ever since *Sandstrom* [1916] showed that ocean circulation without diffusion could only have energy sources from differential heating if the depth of the source of heat lay below the depth of the sink of heat.

4. Combining Partial Mixing and Double Driving

[36] The preceding two sections indicate that if the apparatus has time constants similar to those of the experiments in section 2, and if $\tilde{H}$ is set so that undermixing is expected based on the criteria of section 3, then it is possible to produce doubly driven experiments with partial mixing. This has proven to be correct. As much as possible

the size and buoyancy flux rates for the experiments described in this section were kept close to those of section 2 rather than section 3 due to economic, water supply, and space considerations.

[37] To produce a modified apparatus, a preliminary design configuration, consisting of a small 0.25 m high chamber immersed in a large tank of freshwater, was used to investigate mixing (characterized by $\tilde{H}$) greater than the overmixed limit. This configuration now reverts back to the inverse estuary case, which will be used in the experiments for the remainder of this study. The opening was a 0.03 m wide vertical slot (D = 0.1) in the lower part of the small chamber. Thus, values of $\tilde{H} \leq 2.5$ could be set. Using (7) and (9), the overmixed limit is found to be when

$$\tilde{H}_{ov} = \frac{1}{2} + \left(\frac{w^2}{16c^3D^2}\right)^{1/5}. \tag{13}$$

[38] Using c = 0.12 as before, $\tilde{H}_{ov}$ = 2.2 for this chamber. Visual observations of the interface between salty water and freshwater revealed that for the range $1.25 < \tilde{H} < 2.5$, the interface between the salty water and freshwater was clearly visible and the interface height increased with $\tilde{H}$. As the source approached about $\tilde{H}$ = 2.5 it broke up into an indistinct region.

4.1. The Apparatus for Double Driving With Partial Mixing

[39] The laboratory configuration to be discussed in this section is sketched in Figure 11. The experimental chamber was 0.10 m high, 0.155 m wide and 0.245 m long with walls and top of 0.012 m Plexiglas. The chamber was immersed in a larger reservoir 0.315 m wide, 0.285 m high, and 1.75 m long with freshwater at 20 ± 0.1°C. The chamber was placed on blocks so it was at middepth of the reservoir. The freshwater temperature was maintained by a recirculating thermostatic bath. All measurements of density of water in the small chamber given here are deviations from density of the reservoir. Three vertical walls of the chamber were fixed in place, but the fourth side (of width 0.155 m) had a vertical slot from top to bottom of adjustable widths that were either 0.01, 0.03, or 0.155 m. The top of the chamber had a hole 3 cm from the end opposite the slot through which a 0.0064 m diameter metal tube was placed at a fixed distance below the roof of the chamber. Salt water was pumped into the chamber with a precision pump at a rate of 5×10^{-7} m^3 s^{-1}. The saltwater plume descended and mixed with the surrounding water. The large size of the reservoir insured that the salinity of the experiment remained relatively constant over the course of an experimental run, typically 5–8 hours in duration. However, the salinity did steadily increase by a small amount, and this increase was constantly monitored. In these experiments, the mixing by heating from below was relatively complete while mixing from the salt influx was not. (8) indicates that for the overmixed limit, the three slot widths give $\tilde{H}_{ov}$ = 1.35, 1.83, and 3.0 respectively. Thus, in all cases the mixing was below the overmixed limit and thus in a very crude sense results would apply to the undermixed ocean. The floor of the chamber was made of copper in contact with thermostatically controlled water at a fixed temperature T^*. The other parameters are $\beta S^*/\alpha T^{**} \sim 10$ and an estimate of the ratio of time constants is τ_S/τ_T based on considerations developed in section 2. Oceanic values can be the same or greater, depending on the size of salinity differences, temperature differences, freshwater supply and basin volumes.

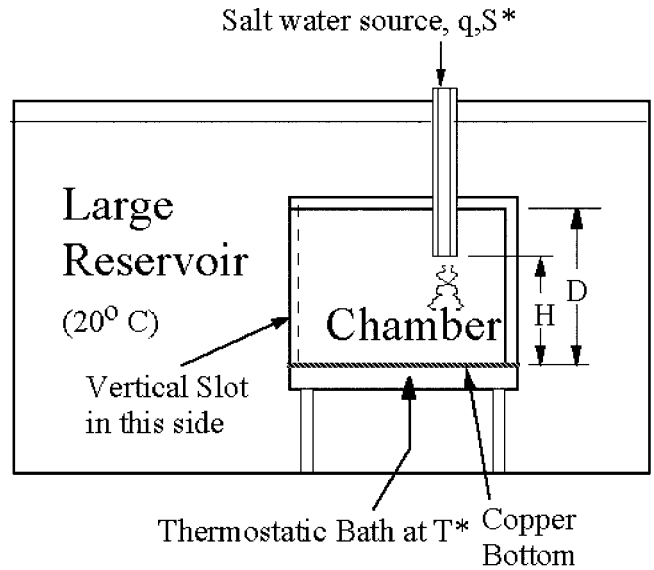

Figure 11. Sketch of the doubly driven apparatus with partial mixing.

[40] The water at the end of the reservoir furthest from the chamber was completely mixed by a thermostat bath at 20°C. Since the salinity source was steady and the reservoir was not flushed, the salinity slowly increased by about 1% of the value of S^* over 24 hours, so the experiment was quasi-steady. The water inside the chamber was observed to attain an exchange flow with the tank after less than 3 hours. Density currents leaving the chamber were free to flow away as supercritical currents that did not return to the chamber.

[41] Measurements of sample density (using a densiometer with samples at 20°C that can be converted to salinity using the equation of state), conductivity (microprobe), temperature (thermistor) and velocity (pellet and dye trajectories of video images) were taken. The pumped salty water was dyed blue so that the darkness of the water indicated salt concentration. Digitized images could produce a distribution of salinity through gray-scale analysis. The flow was visualized from the side by recording the movement of dye on video tape and by taking photographs. Dye was also injected along a vertical column just outside of the slot to record flow through the slot.

4.2. Experimental Observations

[42] Two distinct flow and density configurations were found. A chamber in the T-mode, shown in Figure 12a, had an outflow of hot salty water through roughly the top half of the slot with an inflow of fresh cold reservoir water in the bottom. The water in the interior of the chamber appeared to have a nearly uniform color, hence, relatively constant salinity, so it might be expected that the structure was similar to its counterpart in the well-mixed box experiments.

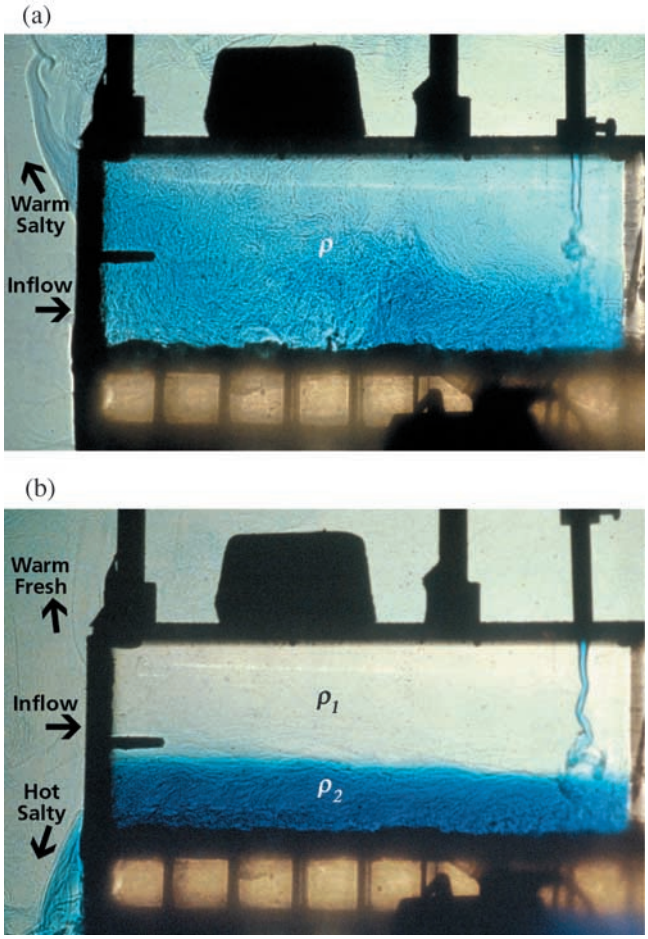

Figure 12. (a) Photograph of a shadowgraph of the chamber, sketched in Figure 11, in the T-mode. (b) In the S-mode. The arrows indicate the flow direction through the slot.

There was some evidence of an arrested salt wedge along the floor of the chamber, with very strong mixing visible at the nose.

[43] A chamber in the S-mode, shown in Figure 12b, had an outflow of hot salty water out of the bottom of the slot, and a second outflow of hot freshwater through the top, with an inflow of cold freshwater at middepth. In the S-mode, the salt water and the freshwater obviously did not thoroughly mix. For example, the depth of the interface remained sharp. Furthermore, the lower layer outflow rate was visibly slower than the outflow in the T-mode. Inside the chamber, the freshwater that entered at mid depth was both mixed into the bottom layer by entrainment into the plume as well as heated from below by the layer of hot salty water. Upon warming, some of this freshwater flowed out of the chamber near the top of the slot with almost no dectectable increase in salinity.

[44] Experiments were conducted for a variety of slot widths, spout heights, and bath temperatures. Multiple equilibria and Stommel transitions were found. Data from the set of experiments that most clearly show multiple equilibria are shown in Figure 13. These experiments had a slot width of 0.03 m and $\tilde{H} \sim 1$. Salinity was determined from samples withdrawn by syringe from the bottom of the chamber at a location 12 cm from the slot. Temperature was recorded with a probe attached above the metal floor (at about 1.5 mm elevation) and data are shown for the maximum and minimum extremes of temperature for the duration of the final observation period of about 15 min. Both the salinity and the temperature varied at the points of measurement, as shown by the scatter of the data in Figure 13. Data were recorded after the experiment had achieved a steady mode for over 2 hours. Typically, the parameters of the experiment in the multiple equilibria range had to be adjusted very gradually in order to obtain the final mode shown. For example, it was necessary to increase T^* in increments less than 0.5°C very slowly during a number of hours to avoid spurious transitions from the T-mode to the S-mode or back. The data were obtained in addition to other exploratory runs for a total of 90 runs, lasting from over 2 hours to days. The scatter arises primarily from variations in salinity and temperature within the layer at any instant rather than measurement uncertainty. Near transition, salinity fluctuations were correlated with temperature fluctuations in such a way that density fluctuations were small. This feature is found in recent models of ocean convection by *Legg and McWilliams* [2000]. Experiments are presently

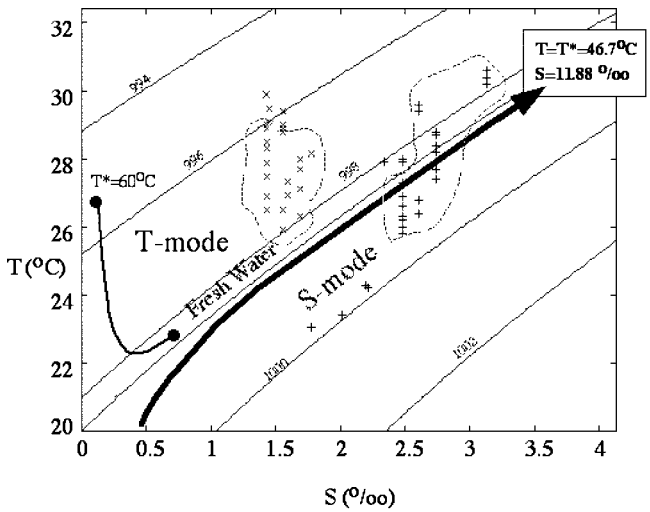

Figure 13. Temperature–salinity diagram of the experimental measurements and overmixed theory. The + symbols indicate values found in the S-mode, the x symbols indicate values found in the T-mode, and the flows in the multiple equilibrium range are enclosed by a dashed curve. The clusters for each mode are distinctly separated. This signifies that a Stommel transition separates the two modes. The S-mode branch from theory is shown on the right as a wide curve that closely follows the density of the reservoir (freshwater at 20°C). The branch extends off the diagram to the upper right to the values shown in the box. The T-mode branch from theory is shown on the left as a curve that starts at the value $T^* = 27.04$°C shown by the solid dot, spirals clockwise, and approaches smaller S and larger T for increasing T^*. The values of the calculation at $T^* = 60$°C terminate the branch shown in this figure although this branch extends for all larger values of T^*. The experimental data are for $29 \leq T^* \leq 36$°C.

being conducted to obtain further data showing the internal T–S structure.

[45] The trajectories of an overmixed theory are shown with the data for comparison. Equations (4) and (5) and the overmixed limit of (7) were combined with precise formulas of the equation of state of water [*Fofonoff and Millard*, 1983] to produce the trajectories. Starting with the measurements that give roughly $S/S^* = 0.13$, (4) was taken together with the imposed volume flux of the salt water of 5×10^{-7} m^3 s^{-1} and a chamber volume of 3.79×10^{-3} m^3 to produce an estimated value of volume flux into the chamber of 3.35×10^{-6} m^3 s^{-1}. Hence, $\tau_s = 7580$s. Then using the value $T/T^* = 9/15$ as shown in the data in Figure 13, with (5), it is estimated that $\tau_T = 755$ s. These time constants are used in conjunction with (4) and (5) and the overmixed exchange formula equation (7) with $\eta = 1/2$ to predict the mode. The overmixed S-mode results were not expected to resemble the layered, undermixed S-mode data in the experiment in section 2.2. This proved to be correct as the S-mode data in Figure 13 do not cluster neatly along the freshwater density curve like the S-mode data in Figure 3. However, the data roughly clustered around the density of freshwater as predicted by the theory, although the transition temperature $T^* = T = 46.7$°C predicted by the theory is significantly greater than the value of experimental transition to only a T-mode of $T^* = 36$°C and $T = 30.6$°C in the experiments. In addition, the trajectories are not aligned with the theoretical trajectory for increasing temperature up to the value $T^* = 36$°C. The T-mode appeared to be overmixed, yet the overmixed theory was not found to adequately predict the T-mode. The experimental T-mode temperatures, and the salinities, were considerably greater than the theory. For example, the top of the theoretical T-mode trajectory for a value of $T^* = 60$°C is shown whereas the greatest value of the data was about $T^* = 36$°C and already the experimental temperature T is greater than theory. The values of T^* for the two Stommel transitions also differed significantly compared to those of the theory. Finally, the volume fluxes predicted by overmixed exchange flow using the equation of state, the geometric values of the chamber opening, and with the observed values of temperature and salinity are an order of magnitude greater than the fluxes estimated from salt conservation considerations. This factor seems to be the cause of the lower values of temperature and salinity from the T-mode theory compared to the data. One possible reason for the differences between experiment and theory for the T-mode, which might seem well mixed, is that the experimental chamber might have large internal variations in T and S which are not measured. It is possible that the salt wedge, visible in Figure 12a, plays an important role. Or perhaps the salt stratification suppresses turbulence in the chamber that could some way alter the temperature time constant in some way.

[46] The relatively small range of control parameter T^* with multiple equilibria is illustrated by the salinity data plotted as a function of T^* in Figure 14. This shows that the range of T^* is about 1°C which contrasts markedly with the range of about 7°C (Figure 3) in the tube experiments of section 2.2.

[47] Experiments revealed that the transition from one mode to another could be readily triggered by temporarily altering the mixing rate. In a number of cases, with $\tilde{H} = 0.8$ the elevation of the plume source was increased when the flow was in the S-mode and within 30 min this triggered the switch to the T-mode, which remained for many hours after restoring the source to $\tilde{H} = 0.8$. In contrast, decreasing the elevation of the source when the flow was in the T-mode

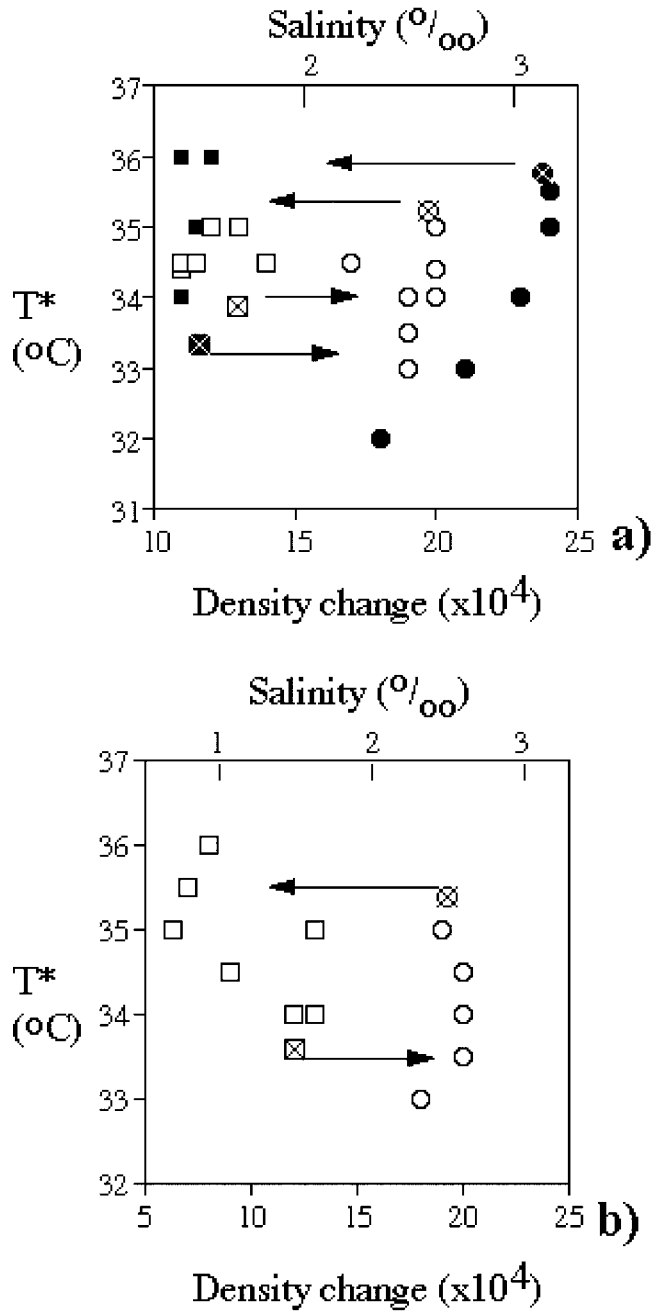

Figure 14. Values of density at 20°C (a proxy for the salinity values shown at the top) for samples in some of the experiments which include the range of multiple equilibrium. (a) Data for an open slot (open symbols) and with the slot blocked from an elevation of 4 to 6 cm (closed symbols) with $\tilde{H} = 1$. The symbols with x and arrows denote modes where T^* was brought to that value but which exhibited a Stommel transition to the other mode. The S-mode data are to the right and T-mode to the left. (b) The same for experiments with $\tilde{H} = 0.8$.

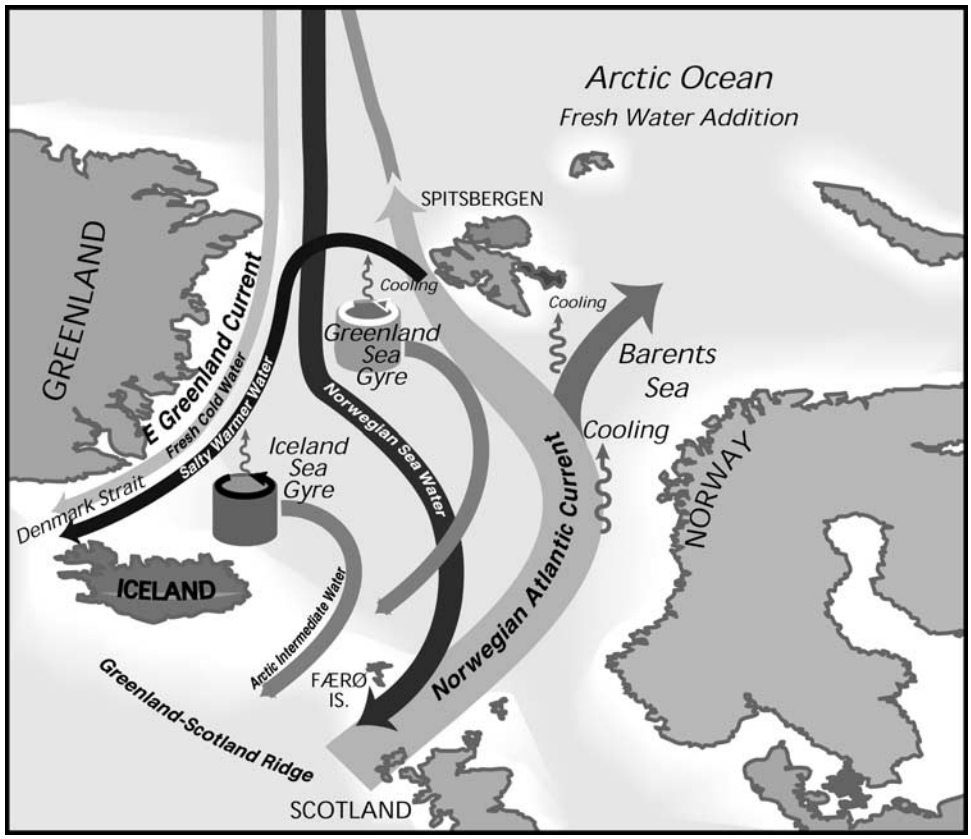

Figure 15. Sketch of the major currents between the North Atlantic and the Nordic Seas [after *Mauritzen*, 1996a, 1996b].

could trigger a switch to the S-mode, which also remained for many hours after restoring the source to the original level.

[48] Many other aspects were explored which had the same qualitative findings as above. For example, experiments with two different slot widths $w = 0.01$ m and 0.15 m gave similar results. A video of a run with T^* set in the hysteresis range shows the S-mode stable for 2 hours. Upon stirring with a handheld rod, the flow settled to a stable T-mode within 10 min. Thus, the flow in the chamber had two stable modes determined by mixing history for the same boundary conditions. Further measurements are now in progress to quantify such results.

[49] At mixing rates of $\tilde{H} \leq 0.8$, transitions were sometimes observed to flows that oscillated irregularly between the T-mode and the S-mode for up to 30 hours. At other times, these fluctuations were not present and their characteristics are not yet documented in detail. In the cases with oscillations, the layer of salt water would slowly get deeper until there was a transition to a T-mode, at which time a new thin salt layer would accumulate on the bottom and initiate a new S-mode. In view of their possible implications for climate, these oscillations deserve careful study.

4.3. Application of the Experiments to the Ocean

[50] In summary, the experiments show that the problem of multiple states, which previously has been considered as only a question of multiple values, is also a problem of multiple structures. In the results so far, the range of hysteresis of the partially mixed experiments is considerably less than the range of the box models. The Stommel transitions are clearly observed but the values of the jumps in temperature and salinity are smaller in the partially mixed experiment than in an overmixed theory.

[51] In addition to the global circulation and the southern ocean stratification, it appears that this result may also apply in a very crude way to the Nordic Seas as sketched in Figure 15. These seas are an undermixed estuary case similar to the Black Sea, with freshwater introduced by continental runoff and more precipitation than evaporation so that a layer of fresher water covers the region. Of course, the opening is much deeper and wider and the exchange flow more complex than the Bosporus two-layer flow. The Norwegian Atlantic current carries saline, relatively warm ($\approx 7°$C) water northward over the Greenland–Scotland ridge from the North Atlantic into the Norwegian/Greenland/Arctic Ocean complex [*Swift and Aagaard*, 1981]. Through a series of alterations, including freshwater addition from the continents and Pacific, four currents remove about the same volume [*Aagaard et al.*, 1981, 1985; *Aagaard and Carmack*, 1989; *Hunkins and Whitehead*, 1992; *Mauritzen*, 1994, 1996a, 1996b]. Two of them (the southward flux through the Baffin Archipelago, and the East Greenland current) contain low salinity water and rafted ice that are needed to complete a freshwater balance. These two movements of freshwater and rafted ice are supplied by water and ice from the upper part of the halocline of the Arctic Ocean. Two other currents, the Denmark Strait overflow [*Ross*,

1984; *Dickson and Brown*, 1994], and the Faeroe channel overflow [*Borenas and Lundberg*, 1988; *Saunders*, 1990] involve the heat budget of deeper water. They bring saltier dense cold water southward over the ridge through the Denmark Straits and through the Iceland–Faeroe channel. They help to complete the heat balance of both the deeper waters, and in conjunction with the above waters, with the heat budget of the entire region. Both currents are sources of the lower North Atlantic deep water, and contribute to global circulation.

[52] The S-mode in the limited mixing experiments resembles the present state of the Arctic Ocean and the S-mode exchange flows resemble exchange flows with the North Atlantic. Note that the laboratory experiments are an inverse estuary case and the Arctic is the estuary case. In the experiment, water of intermediate density flows into the chamber. This is an analog of the North Atlantic current (sometimes called the Gulf Stream in Europe) that brings warm water from the North Atlantic into the Greenland/Norwegian Sea. The laboratory outflow is comprised of two currents, one with altered temperature and higher salinity, (an analog of the Baffin and upper East Greenland freshwater currents), and the other with the same salinity and altered temperature (an analog of the deep cold overflows). A layer of salt water lies in the upstream basin (an analog of the Arctic pycnocline). The experiments here show that increased mixing alone can trigger a transition to the T-mode. Whether this is within the range of possibility of the Arctic Ocean is unknown.

5. Concluding Summary

[53] It is straightforward to produce laboratory studies with flows driven by both thermal and salinity differences and with partial mixing in such flows. The results are compared with common box model results. In the classic T–S box problem, an experimental chamber is heated from below, exposed to a steady flux of salt water from above through a tube, and laterally connected to a reservoir of fresh isothermal water. Two locally stable modes of circulation are found the T-mode and the S-mode with hysteresis and Stommel transitions between the two modes being decreased as mixing decreased. Experiments find a three-layer structure for the S-mode and a two-layer structure for the T-mode. Stommel transitions are still present, while hysteresis is considerably smaller than in the fully mixed box models. Results are consistent with the notion that the Arctic Ocean is presently undermixed and in the layered S-mode.

[54] **Acknowledgments.** The National Science Foundation, Ocean Sciences Division, under grants OCE-9733063 and OCE-0081179 and the Office of Naval Research under grant N00014-97-1-0195 gave support for the laboratory studies. International travel was supported by NSF grant INT 9724825 and NSF-CONACYT (ref. E 120.1279). The 1997 Geophysical Fluid Dynamics Summer Study Program (for M.L.E.T.) was supported by NSF grant OCE-9314484. Woods Hole Oceanographic Institution contribution 9921.

References

Aagaard, K., and E. C. Carmack, The role of sea ice and other fresh water in the Arctic circulation, *J. Geophys. Res.*, *94*, 14,485–14,498, 1989.

Aagaard, K., L. K. Coachman, and E. Carmack, On the halocline of the Arctic Ocean, *Deep Sea Res.*, *28A*, 529–545, 1981.

Aagaard, K., J. H. Swift, and E. C. Carmack, Thermohaline circulation in the Arctic Mediterranean seas, *J. Geophys. Res.*, *90*, 4833–4846, 1985.

Armi, L., and D. Farmer, Maximal two-layer exchange through a contraction with barotropic net flow, *J. Fluid Mech.*, *164*, 27–51, 1986.

Borenas, K. M., and P. A. Lundberg, On the deep-water flow through the Faroe bank channel, *J. Geophys. Res.*, *93*, 1281–1292, 1988.

Brocard, D. N., and D. R. F. Harleman, Two-layer model for shallow horizontal convective circulation, *J. Fluid Mech.*, *100*, 129–146, 1980.

Broecker, W. S., and G. H. Denton, The role of ocean–atmosphere reorganizations in glacial cycles, *Geochim. Cosmochim. Acta*, *53*, 2465–2501, 1989.

Dickson, R. R., and J. Brown, The production of North Atlantic Deep Water: Sources, rates and pathways, *J. Geophys. Res.*, *99*, 12,319–12,341, 1994.

Faller, A., Sources of energy for the ocean circulation and a theory for the mixed layer, in *Proceedings Fifth U.S. National Congress of Applied Mechanics, Minneapolis, MN*, pp. 651–672, Am. Soc. of Mech. Eng., New York, 1966.

Fofonoff, N. P. and R. C. Millard Jr., Algoriths for computation of fundamental properties of seawater, UNESCO paper in Marine Science 44, Div. of Mar. Sci., UNESCO, Place de Fontenoy, 75700 Paris, France, 1983.

Gordon, A. L., Two stable modes of Southern Ocean Winter Stratification, in *Deep Convection and Deep Water Formation in the Oceans*, edited by P. C. Chu and J. C. Gascard, pp. 17–35, Elsevier Sci., New York, 1991.

Gordon, A. L., and B. A. Huber, Southern Ocean winter mixed layer, *J. Geophys. Res.*, *95*, 11,655–11,672, 1990.

Grimm, T., and T. Maxworthy, Buoyancy-driven mean flow in a long channel with a hydraulically constrained exit condition, *J. Fluid Mech.*, *398*, 155–180, 1999.

Hearn, C. J., and H. S. Sidhu, The Stommel model of shallow coastal basins, *Proc. R. Soc. London*, *A455*, 3997–4011, 1999.

Huang, R. X., Mixing and energetics of the oceanic thermocline circulation, *J. Phys. Oceanogr.*, *29*, 727–746, 1999.

Hunkins, K., and J. A. Whitehead, Laboratory simulation of exchange through Fram Strait, *J. Geophys. Res.*, *97*, 11,299–11,321, 1992.

Legg, S., and J. C. McWilliams, Temperature and salinity variability in heterogeneous oceanic convection, *J. Phys. Oceanogr.*, *30*, 1188–1206, 2000.

Marotzke, J., Ocean models in climate problems, in *Ocean Processes in Climate Dynamics: Global and Mediterranean Examples*, edited by P. Malanotte-Rizzole and A. R. Robinson, pp. 79–109, Kluwer Acad., Norwell, Mass., 1994.

Mauritzen, C., A study of the large scale circulation and water mass formation in the Nordic Seas and Arctic Ocean, Ph.D. thesis, *WHOI Tech. Rep. WHOI-93-53*, Woods Hole Oceanogr. Inst.–Mass. Inst. of Technol. Joint Program, 1994.

Mauritzen, C., Production of dense overflow waters feeding the North Atlantic across the Greenland–Scotland Ridge, part 1, Evidence for a revised circulation scheme, *Deep Sea Res.*, *43*, 807–835, 1996a.

Mauritzen, C., Production of dense overflow waters feeding the North Atlantic across the Greenland–Scotland Ridge, part 2, An inverse model, *Deep Sea Res.*, *43*, 769–806, 1996b.

Morton, B. R., S. G. Taylor, and J. S. Turner, Turbulent gravitational convection from maintained and instantaneous sources, *Proc. R. Soc. London*, *A234*, 1–23, 1956.

Ozsoy, E., U. Unluata, and Z. Top, The evolution of Mediterranean water in the Black Sea: Interior mixing and material transport by double diffusive intrusions, *Prog. Oceanogr.*, *31*, 275–320, 1993.

Polzin, K. L., K. G. Speer, J. M. Toole, and R. W. Schmitt, Intense mixing of Antarctic bottom water in the equatorial Atlantic Ocean, *Nature*, *380*, 54–57, 1996.

Polzin, K. L., J. M. Toole, J. R. Ledwell, and R. W. Schmitt, Spatial variability of turbulent mixing in the abyssal ocean, *Science*, *276*, 93–96, 1997.

Rahmstorf, S., and Ganapolski, Simple theoretical model may explain apparent climate instability, *J. Clim.*, *12*, 1349–1352, 1999.

Ross, C. K., Temperature-salinity characteristics of the "overflow" water in Denmark Strait during "OVERFLOW 73", *Rapp. P. V. Reun. Cons. Int. Explor. Mer.*, *185*, 111–119, 1984.

Sandstrom, J. W., Meteorologische Studien im schwedischen Hochgebirge, *Goteb. K. Vetensk. Vitterh.-Samh. Handl.*, *4, 22*(2), 48, 1916.

Saunders, P. M., Cold outflow from the Faroe bank channel, *J. Phys. Oceanogr.*, *20*, 29–43, 1990.

Schmitt, R., Double-diffusion in oceanography, *Annu. Rev. Fluid Mech.*, *26*, 255, 1994.

Stommel, H., Thermohaline convection with two stable regimes of flow, *Tellus*, *13*, 224–230, 1961.

Stommel, H., and H. G. Farmer, Abrupt change in width in two-layer open channel flow, *J. Mar. Res.*, *11*, 205–214, 1952.

Stommel, H., and H. G. Farmer, Control of salinity in an estuary by a transition, *J. Mar. Res.*, *12*, 13–20, 1953.

Sverdrup, H. U., M. W. Johnson, and R. H. Fleming, *The Oceans*, 1087 pp., Prentice-Hall, Old Tappan, N. J., 1942.

Swift, J. H., and K. Aagaard, Seasonal transitions and water mass formation in the Iceland and Greenland Seas, *Deep Sea Res.*, *28A*, 1107–1129, 1981.

Timmermans, M. L. E., Hydraulic control and mixing in a semi-enclosed reservoir, *Geophys. Fluid Dyn. Summer Study Program Tech. Rep. WHOI-98-09*, 1998.

Turner, J. S., *Buoyancy Effects in Fluids*, Ch. 8, Cambridge Univ. Press, New York, 1973.

Weaver, A. J., C. M. Bitz, A. F. Fanning, and M. M. Holland, Thermohaline circulation: High-latitude phenomena and the difference between the Pacific and Atlantic, *Annu. Rev. Earth Planet. Sci.*, *27*, 231, 1999.

Whitehead, J. A., Thermohaline ocean processes and models, *Annu. Rev. Fluid Mech.*, *27*, 89–114, 1995.

Whitehead, J. A., Multiple states in doubly-driven flow, *Physica D*, *97*, 311–321, 1996.

Whitehead, J. A., Multiple T-states for estuaries, shelves and marginal seas, *Estuaries*, *21*, 278–290, 1998.

S. N. Bulgakov, J. F. A. Medina, and A. M. Zatarain, Institute of Astronomy and Meteorology, University of Guadalajara, Av. Vallarta 2602, Sector Juares, C.P. 44100, Guadalajara, Jalisco, Mexico.

W. G. Lawson, 54-1611, Massachusetts Institute of Technology, Cambridge, MA 02139, USA.

J. Salzig and J. A. Whitehead, Department of Physical Oceanography, Woods Hole Oceanographic Institution, MS 21, 360 Woods Hole Road, Woods Hole, MA 02543, USA. (jwhitehead@whoi.edu)

M. L. E. Timmermans, Institute of Theoretical Geophysics, DAMTP, University of Cambridge, Cambridge, CB3 9EW, UK.